Geophysical Research Letters

RESEARCH LETTER
10.1029/2018GL080410

Hydrothermal Heat Enhances Abyssal Mixing in the Antarctic Circumpolar Current

Stephanie M. Downes[1], Bernadette M. Sloyan[2], Stephen R. Rintoul[1,2], and John E. Lupton[3]

[1]Antarctic Climate and Ecosystems Cooperative Research Centre, University of Tasmania, Hobart, Tasmania, Australia, [2]Commonwealth Scientific and Industrial Research Organisation Oceans and Atmosphere, and Centre for Southern Hemisphere Oceans Research, Hobart, Tasmania, Australia, [3]NOAA Pacific Marine Environmental Laboratory, Newport, OR, USA

Abstract Upwelling in the world's strongest current, the Antarctic Circumpolar Current, is thought to be driven by wind stress, surface buoyancy flux, and mixing generated from the interaction between bottom currents and rough topography. However, the impact of localized injection of heat by hydrothermal vents where the Antarctic Circumpolar Current interacts with mid-ocean ridges remains poorly understood. Here a circumpolar compilation of helium and physical measurements are used to show that while geothermal heat is transferred to the ocean over a broad area by conduction, heat transfer by convection dominates near hydrothermal vents. Buoyant hydrothermal plumes decrease stratification above the vent source and increase stratification to the south, altering the local vertical diffusivity and diapycnal upwelling within 500 m of the sea floor by an order of magnitude. Both the helium tracer and stratification signals induced by hydrothermal input are advected by the flow and influence properties downstream.

Plain Language Summary Oceans soak up over 90% of the energy from global warming and regulate the Earth's climate. Along the ocean floor, more than 630 hydrothermal vents are spewing superhot plumes of water out of cracks in the Earth's crust. At the same time, the ocean floor is being gently warmed by magma under the Earth's crust, known as geothermal heating. But few research studies have measured and compared the effect of both hydrothermal and geothermal heat sources on major ocean currents. In this study, we analyzed over 3 million temperature, salinity and helium data points across the Southern Ocean that houses the world's strongest current, the Antarctic Circumpolar Current. The aim of the study was to determine how hydrothermal heat and geothermal heat affect the already-turbulent circulation of this current. The study finds that the circulation within a few hundred meters of hydrothermal vents in the Antarctic Circumpolar Current increases by tenfold, compared to circulation around it. The authors show, for the first time, that hydrothermal vents play a major role in ocean currents at a local scale (more than geothermal heat), and this role cannot be ignored, as has previously been done in climate modeling and ocean circulation research.

Key Points:
- Heat input by hydrothermal vents has a strong local influence on Southern Ocean circulation
- Hydrothermal heat reduces stratification over vents and increases it to the south, altering abyssal mixing rates
- Both hydrothermal heating and geothermal heating need to be accounted for in studies of abyssal circulation and mixing

Supporting Information:
- Figure S1
- Figure S2
- Figure S3
- Text S1
- Text S2

Correspondence to:
S. M. Downes,
s.downes@utas.edu.au

Citation:
Downes, S. M., Sloyan, B. M., Rintoul, S. R., & Lupton, J. E. (2019). Hydrothermal heat enhances abyssal mixing in the Antarctic Circumpolar Current. *Geophysical Research Letters*, *46*, 812–821. https://doi.org/10.1029/2018GL080410

Received 15 SEP 2018
Accepted 17 DEC 2018
Accepted article online 2 JAN 2019
Published online 18 JAN 2019

1. Introduction

The estimated globally averaged 0.064–0.085 W/m^2 conductive geothermal heat flux emanating from the seabed (Davies & Davies, 2010; Hamza et al., 2008) does not fully account for the transfer of heat from the solid Earth to the deep ocean. The geothermal heat input is dominated by the contribution from the 71,000-km-long chain of relatively young spreading mid-ocean ridges, where the geothermal heat flux is up to an order of magnitude larger than values typical of the older abyssal plains (Anderson et al., 1977; Davies & Davies, 2010). In addition, more than 630 known hydrothermal vents are found on mid-ocean ridges (Baker, 2017). The superhot plumes expelled from these vents entrain background fluid as they rise, while injecting the deep ocean with chemicals, buoyancy, and momentum (Baker et al., 2012; Bemis et al., 1993). Convective hydrothermal plumes transfer heat vertically, alter local vorticity, and establish rotating circulations as they rise (Speer & Helfrich, 1995). We define this convective heat flux as "hydrothermal heat." A recent idealized model study (Barnes et al., 2017) showed that the hydrothermal heat flux (prescribed as a vertical velocity at the bottom boundary) can increase vertical advection in the deep ocean by 35%, adding to the contribution

from conductive geothermal heat fluxes. However, obtaining widespread measurements of this convective flux has proven challenging, given the small surface area and episodic nature of these intense plumes.

Several model studies have shown that the nonuniformly distributed conductive geothermal heat flux weakens the deep ocean stratification, increasing the deep meridional overturning circulation by 25–50% (Adcroft et al., 2001; Hofmann & Morales Maqueda, 2009; Mashayek et al., 2013), transforming 5 to 8 Sv of Antarctic Bottom Water (AABW) to lighter waters (de Lavergne et al., 2016; Emile-Gaey & Madec, 2009), and decreasing Antarctic Circumpolar Current (ACC) transport by approximately 5 Sv (Downes et al., 2016). The associated modeled temperature anomalies of up to 0.5 ° C induced along the global ocean floor can be upwelled toward the surface, particularly in the Southern Ocean (Downes et al., 2016), increasing poleward heat transport by ~10% (Emile-Gaey & Madec, 2009). Piecuch et al. (2015) show that the modeled response in the global mean steric height to geothermal heating is an order of magnitude larger in the Southern Ocean.

While there is growing recognition of the influence of geothermal heat flux on ocean circulation, the contribution from hydrothermal heat flux has received much less attention. Here we focus on the impact of hydrothermal heating on the Southern Ocean. The ACC, the world's largest ocean current, circles the Antarctic continent with a transport of 130 to 170 Sv (Chidichimo et al., 2014; Cunningham et al., 2003). The ACC is steered and interacts with topography along its circumpolar path (Rintoul & Naveira Garabato, 2013; Rintoul, 2018). Within the ACC, the interaction of bottom currents with rough topography results in the production of lee waves and, where they break, increased dissipation of kinetic energy (Kunze et al., 2006; Naveira Garabato et al., 2004). Enhancement of turbulent mixing over rough topography and mid-ocean ridges in the ACC region is well known, with diapycnal diffusion strongly correlated with topographic roughness (Naveira Garabato et al., 2004). Vertical mixing within approximately 1,000 m of the ocean floor over mid-ocean ridges and other topographic features has been observed to be 2 to 3 orders of magnitude larger than the $\sim 10^{-5}$ m^2/s rate typical of abyssal plains (Naveira Garabato et al., 2004, 2007; Kunze et al., 2006; Sloyan, 2005, 2006; Waterhouse et al., 2014). However, the contribution from hydrothermal and geothermal seabed sources as the ACC flows above and along five mid-ocean ridge chains (Figure 1a) has not yet been investigated. We show here that buoyant hydrothermal plumes can change local stratification, and therefore vertical diffusivity.

Observations of the Southern Ocean are sparsely distributed in both time and space, with chemical tracer data that are used to identify hydrothermal sources even more limited. In this study, we compile over 40 years of tracer data to explore the impact of hydrothermal heat on localized upwelling and mixing of deep waters within the ACC. We show, for the first time, that hydrothermal heating enhances vertical diffusion hundreds of meters above the seafloor within the Lower Circumpolar Deep Water (LCDW) and AABW water mass classes in the ACC. We identify regions where we observe, and should observe, the role of hydrothermal and geothermal heating in ACC dynamics.

2. Methods

2.1. Southern Ocean Data and Selected Transects

The conductive geothermal heat flux data set used here (Davies & Davies, 2010), Q_{geo}, is a combined empirical and observed estimate using 38,374 measurements. The data set is available on a 1° × 1° grid and has a conservative error estimate of ±30 mW/m^2. This error estimate does not impact the interpretation of our results.

We used data from 20 hydrographic voyages: 3 from the 1970s, 14 from the 1990s, and the remainder from the 21st century (Figure 1a). The data from all but one voyage are sourced from the Climate Variability and Predictability Program and Carbon Hydrographic Office (https://cchdo.ucsd.edu/) repository of bottle data (helium) and conductivity-temperature-depth (CTD) measurements for temperature and salinity. We also include data from regional Southern Ocean voyages (Hahm et al., 2015; courtesy of Drs. Doshik Hahm and Edward Baker). This study analyzes 3,683,260 CTD data points of temperature and salinity, interpolated onto neutral density surfaces (Jackett & McDougall, 1997). We use 87,627 helium measurements across the Southern Hemisphere to assess mid-ocean ridges within and north of the Southern Ocean. All analyzed data underwent quality control as it was processed, and we removed all data flagged to be suspicious. The δ^3He is estimated using ^{3}He and ^{4}He data (Clarke et al., 1970): $\delta^3\mathrm{He} = 100 * ((^3\mathrm{He}_s/^4\mathrm{He}_s)/(^3\mathrm{He}_a/^4\mathrm{He}_a) - 1)$, where s denotes helium from the hydrographic sample and a from the

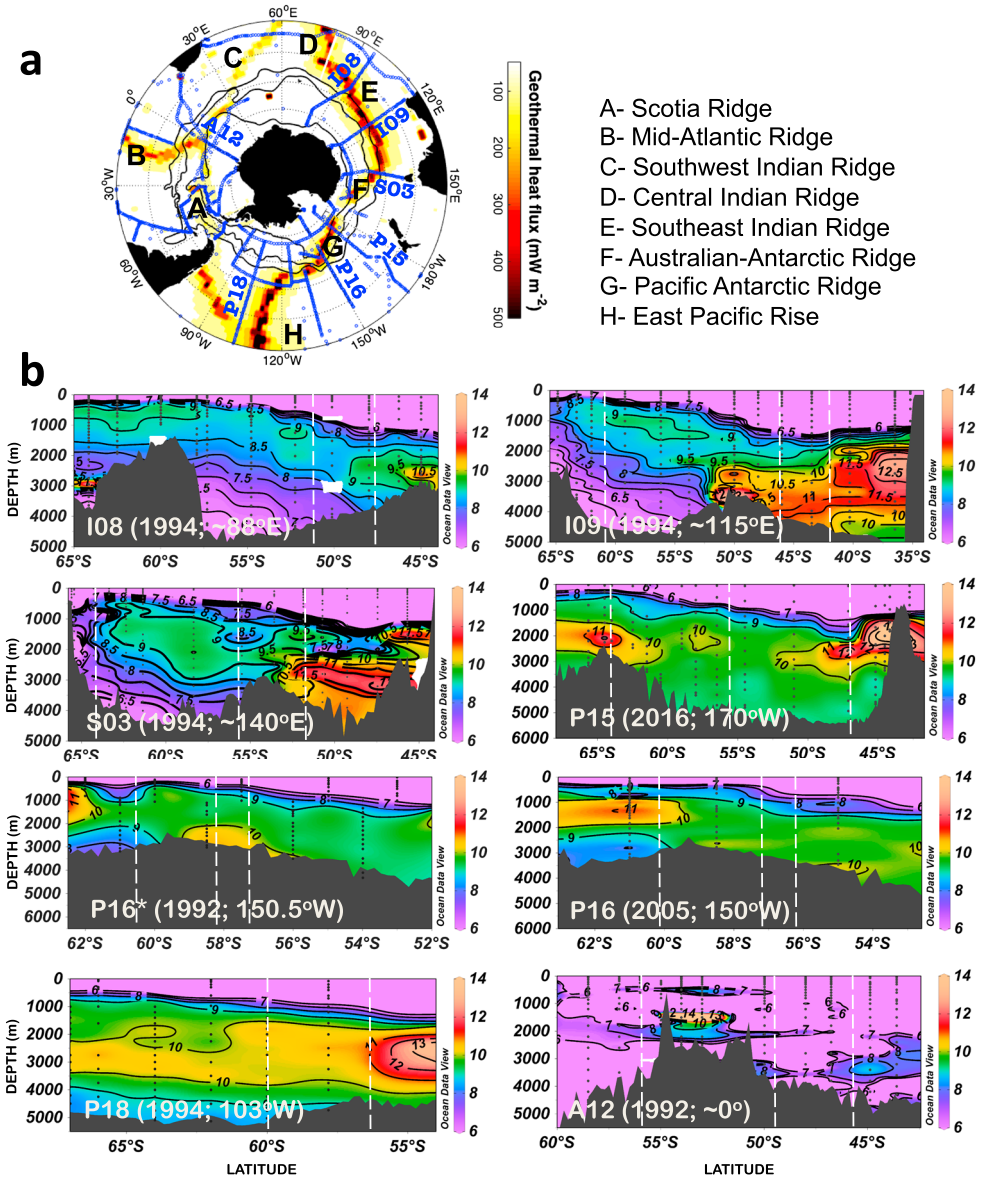

Figure 1. (a) The geothermal heat flux (mW/m^2; Davies and Davies, 2010) overlaid with stations used in this study (blue circles). Transects of interest are noted in blue text and major mid-ocean ridge segments in black lettering, with the legend on the right. (b) Sections corresponding to the transects highlighted in (a). Colors and contours are δ^3He (%). White dashed lines indicate latitudes of the Antarctic Circumpolar Current fronts (left to right: Southern Boundary Front, Polar Front, and Subantarctic Front). The P18 and I08 transects end before the Antarctic Circumpolar Current southern boundary).

atmosphere. The helium data were linearly interpolated onto a regular 1° × 1° grid and mapped using the M_map tool (https://www.eoas.ubc.ca/~rich/map.html).

What makes helium (δ^3He) an extremely useful tracer is that its oceanic source is restricted to hydrothermal circulation; it is a passive tracer unaffected by changes in ocean buoyancy at the source, and it provides a natural tracer for water mass circulation. In this study, we use δ^3He as a proxy for hydrothermal heat; the two are not linearly correlated (Lupton et al., 1999), but a distinct δ^3He signature at the sea floor implies the existence of hydrothermal heat. Hydrothermal vents have a helium ratio (^{3}He/^{4}He) that is almost an order of magnitude higher than the atmosphere (Krylov et al., 1974; Lupton & Craig, 1975), producing a δ^3He signature of 5% to over 40% (Hahm et al., 2015; Lupton et al., 2004; Lupton & Craig, 1975; Rüth et al., 2000; Saito et al., 2013; Srinivasan et al., 2004; Well et al., 2001, 2003). The strongest helium signatures are found in

the Pacific Ocean, where there is a large East Pacific Rise fingerprint of δ^3He > 30% (see also Lupton, 1998). The lowest signatures are found in the Atlantic basin, given that the Mid-Atlantic Ridge expels δ^3He of up to 20% (see also Saito et al., 2013; Well et al., 2003), with the helium signatures from Indian mid-ocean ridges in the 10–20% range (see also Srinivasan et al., 2004). We focus on eight GO-SHIP hydrographic transects in this study (A12, I08, I09, S03, P15, P16*, P16, and P18; Figure 1), chosen to cover regions of high and low geothermal heat across mid-ocean ridges and abyssal plains intersecting the ACC in all major basins.

2.2. Calculation of Stratification, Vertical Mixing, and Upwelling Rates

While helium provides an unambiguous indication of hydrothermal sources, other processes can influence circulation and stratification near the sea floor. We thus compare the distributions of stratification (a measure of the vertical density gradient) and of hydrothermal activity along the ocean floor. The stratification and vertical diffusivity estimates used herein are those of Sloyan (2005). Stratification (the squared Brunt-Vaisala frequency, N; units of s^{-1}) is calculated as $N^2 = -(g/\rho)/\partial\rho/\partial z$, where $g = 9.8$ m/s^2 is the acceleration due to gravity, ρ is potential density, and z is depth. We estimate N^2 using high-resolution CTD data spaced approximately every 2 dbar. Given that topography can change dramatically between stations, when discussing the impact of hydrothermal and geothermal heating on the local circulation near the ocean floor, we take the maximum N^2 within the bottom 150 m at each station. This depth range lies within the typical rise height of hydrothermal plumes.

The strain-based vertical diffusion, $\kappa = \Gamma\frac{\epsilon}{N^2}$, where ϵ is the dissipation of turbulent kinetic energy and the mixing efficiency, $\Gamma = 0.2$. The dissipation rate is a function of the fine-scale strain, $\xi_z = (N^2 - \overline{N^2})/\overline{N^2}$, where the N^2 is the fine-scale stratification, defined over a 40-m vertical range, whereas the mean stratification ($\overline{N^2}$) is defined over a 500-m-depth range. The uncertainty in the diffusivity estimates used in this study is a factor of 2 to 5, based on the measurement errors, data availability, and assumptions about the shear to strain ratio (Sloyan, 2005). This error is small compared to the order of magnitude difference between the high vertical diffusivity rates associated with hydrothermal heating and the rates at adjacent data points. Here we want to assess how hydrothermal and geothermal heat affect mixing away from the seabed (where frictional effects come into play), above the typical plume rise height and within the large-scale circulation. Hence we estimate κ at approximately 300 and 500 m above the seabed. We note that the vertical diffusivities can be much smaller at other depths within 500 m of the seabed along some transects, and our depth range choice is to highlight key signatures. We perform a simple estimate of the impact of hydrothermal plumes on the diapycnal upwelling rate, $w* = (1/N^2)(\partial(\kappa \times N^2)/\partial z)$ (Naveira Garabato et al., 2007).

3. Results

3.1. Geothermal Heat Versus Hydrothermal Heat

While several studies have used the chemical signatures of hydrothemal plumes as a passive tracer to identify pathways of deep circulation (e.g., Downes et al., 2012; Lupton & Craig, 1975; Veirs et al., 1999; Winckler et al., 2010), few have quantified the regional impact of the expelled heat on the background flow. Hydrothermal plumes are located at the seabed within the LCDW and AABW water mass layers ($\gamma^n \geq 28.1$ kg/m^3), and the δ^3He varies significantly across and within the major ocean basins within these density layers (Figure S1 in the supporting information). To summarize the influence of hydrothermal and geothermal heating on the Southern Ocean large-scale circulation, we need to assess multiple transects across this region. Some sections (Figure 1b) show helium signals from ACC-sourced vents that have been advected downstream (e.g., P16 and P18 between the Polar Front and southern ACC boundary; Downes et al., 2012). Half of the eight chosen transects show high δ^3He hydrothermal vent signatures along the seabed *within* the ACC region, namely, P16* at 150.5° W, P15 at 170° W, S03 at approximately 140° E, and I09 at approximately 115° E. Hydrothermal plumes are evident between the Polar Front and ACC southern boundary along the Pacific-Antarctic Ridge crest (P16*; δ^3He = 10.5%; 59.5° S), at the southern boundary of the ACC along the same ridge segment (P15; δ^3He = 13%; 64.5° S), and within the Polar Front to Sub-Antarctic Front region along the Southeast Indian Ridge (S03; δ^3He = 10%; 54° S and I09; δ^3He = 14%; 50° S). We also find δ^3He contributions from ridges outside of the Southern Ocean, including the Central Indian Ridge [e.g., I08], East Pacific Rise [e.g., P16*, P16, and P18], and Mid-Atlantic Ridge [e.g., A12].

The superhot fluid expelled from vents of over 100 ° C (Baker et al., 1995; Haase et al., 2009) entrains cooler background fluid as it rises, and thus, the strongest influence of the hydrothermal heat is localized, despite the tracer signal often spreading thousands of kilometers from the vent (Downes et al., 2012; Gnanadesikan

et al., 2015; Lupton, 1998; Lupton & Craig, 1975; Winckler et al., 2010). The ascent of buoyant hydrothermal plumes convectively mixes the overlying water column, producing a stratification minimum over the vent. Stratification minima near the seafloor along each transect are not solely associated with geothermal and/or hydrothermal activity. However, where there are high δ^3He/high Q_{geo} signals along the seafloor, we find that the associated stratification minima rises several hundred meters above the seafloor in a plume-like distribution.

While the change in stratification is largest near the plume source, the resulting δ^3He and stratification signals are advected downstream at or above the plume rise height (~200 m). A fortuitous example is along P16 (Figures 1b and S2, bottom row). There are two occupations of this transect shown here, separated by half a degree of longitude, namely, P16* at 150.5° W (1992) and P16 at 150° W (2005). The former shows a clear hydrothermal δ^3He plume at the Pacific-Antarctic Ridge crest near 59° S. Along the latter P16 150° W transect (and for repeat occupations since 2005), the δ^3He signature is significantly smaller along the ridge crest, implying that the plume expelled at P16* (150.5° W) has likely been advected eastward along the southern half of the ACC to P16 (150° W; Downes et al., 2012). Both the P16* and P16 sections have high geothermal heat input in the ACC region (Figure 1a); however, as shown below, the impact of hydrothermal heat on stratification and mixing is larger at P16*, where a distinct maximum in δ^3He is observed, than downstream at P16, where no distinct maximum is observed.

3.2. Enhanced Deep Ocean Mixing in the ACC

In Figure 2 we focus on the key signatures nearest to the ocean floor to better capture changes in stratification closest to and associated with plume sources. We use the helium tracer as a proxy for hydrothermal heat (blue curves) and a geothermal heat flux data set as an estimate of the conductive heat flux contribution (Davies & Davies, 2010; Q_{geo}; red dots for fluxes greater than 200 mW/m^2) to identify the impact of hydrothermal/geothermal heat on local stratification (black curves), and thus isopycnal gradient. Both convective (as inferred from high helium) and conductive sources of heat contribute to reducing the stratification along the already weakly stratified bottom of the ocean.

What is most clear near the latitude of the high helium (and sometimes also high geothermal) signature is the maxima in stratification, particularly along I09, P15 and P16* transects. As hydrothermal heat is injected from the sea floor the water column is mixed by buoyant convection and local density decreases directly above the source. This deepening enhances the isopycnal tilt. As the background flow is associated with isopycnals that shoal to the south, convective mixing by the plume causes isopycnals to deepen and shift to the south, resulting in bunching of isopycnals and enhanced stratification immediately south of the plume. That is, injection of hydrothermal heat decreases stratification over the source and increases stratification immediately to the south. The increase in stratification can be as much as 11–25 $\times 10^{-5}$ s^{-2}, almost an order of magnitude larger than found at surrounding stations. The enhanced steepening of isopycnals over the hydrothermal vents occurs in the LCDW and AABW layers ($\gamma^n = 28.1, 28.15$, and 28.2 kg/m^3 in Figure S2).

While interaction of the flow with rough topography can also alter stratification near the seabed (Figure 2 and Sloyan, 2006), and hence we do not expect all stratification maxima to coincide with hydrothermal plumes, maxima in helium along each transect are aligned with a local maximum in stratification, both within (I09, P15 and P16*) and outside of (I08 and S03) the ACC. These maxima in some cases are aligned with high geothermal heat fluxes, that is, high conductive and high convective heat input can occur in the same location. Along P16 (the 2005 occupation), there is no hydrothermal source, and we do not observe a significant a change in stratification, implying that a geothermal heat source alone is not enough to drive large stratification changes near the sea floor.

In Figure 3, we show local mixing rates between 300 and 500 m above the sea floor as function of latitude for six sections across the ACC. We choose this range as it is above the typical plume rise height and because mixing near the sea bed typically exceeds 10^{-3} m^2/s, making it difficult to separate impacts of plumes. The vertical diffusivity rates in Figure 3 range from less than 10^{-5} to 10^{-3} m^2/s, agreeing well with studies that have diagnosed diffusivity along rough topography and mid-ocean ridges (Waterhouse et al., 2014). Our estimates are also in good agreement with the 1 to 40 $\times 10^{-4}$ m^2/s found along the East Scotia Ridge (including a 100 mW/m^2 geothermal heat flux in the estimate; Heywood et al., 2002). Mixing is elevated relative to background levels across most of the ACC, reflecting mixing driven by lee waves produced by interaction of strong deep flows with rough topography. Figure 3 illustrates that mixing is further enhanced in some locations where hydrothermal heat input and stratification are high (yellow dots).

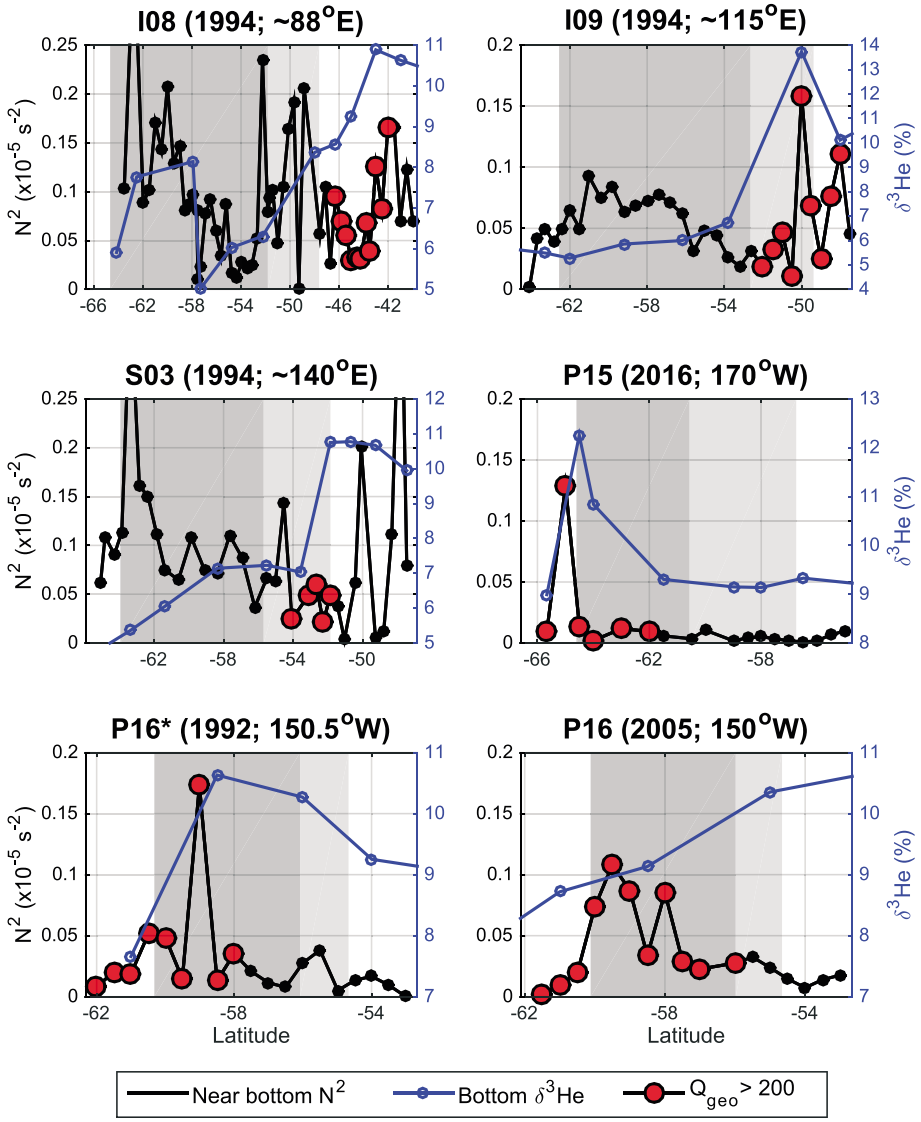

Figure 2. Stratification (N^2; $\times 10^{-5}$ s^{-2}) within 150 m of the seabed at six of the eight focus sections (excluding P18 and A12; see text). Black dots indicate where data are available. Overlaid red dots indicate the region where geothermal heat flux (Davies and Davies, 2010) is greater than 200 mW/m^2. The δ^3He (%) near the ocean floor is in blue. Dark gray shaded region is the southern Antarctic Circumpolar Current boundary to the Polar Front, with the lighter gray shaded region the Polar Front to Sub-Antarctic Front.

A number of processes affect mixing intensity near the sea floor in the ACC, making the relationship between topography, heat input, and mixing a complicated one (i.e., intense mixing sometimes occurs in the absence of high geothermal/hydrothermal heat input, and high geothermal/hydrothermal heat input is not always associated with elevated mixing). For example, the meridional change in bathymetry (gray curves) in Figure 3 aligns well with the high vertical mixing and along many of the transects.

Three key results are found on those sections where the ACC encounters hydrothermal sources (I09, P15, and P16*). The first is that maxima in the vertical diffusivity within 300 to 500 m of the seabed are colocated with hydrothermal sources and a maxima in stratification near the sea floor (Figure 2 and yellow dots in Figure 3). The P16 section, which does not show evidence of a hydrothermal plume, shows an anomaly in the stratification that is half that of P16* (Figure 2; bottom row) and a vertical diffusivity (Figure 3f) that is more than an order of magnitude smaller than along P16* (Figure 3e). This difference between the two P16 sections, only separated by half a degree of longitude, reinforces the notions that high Q_{geo} alone does not

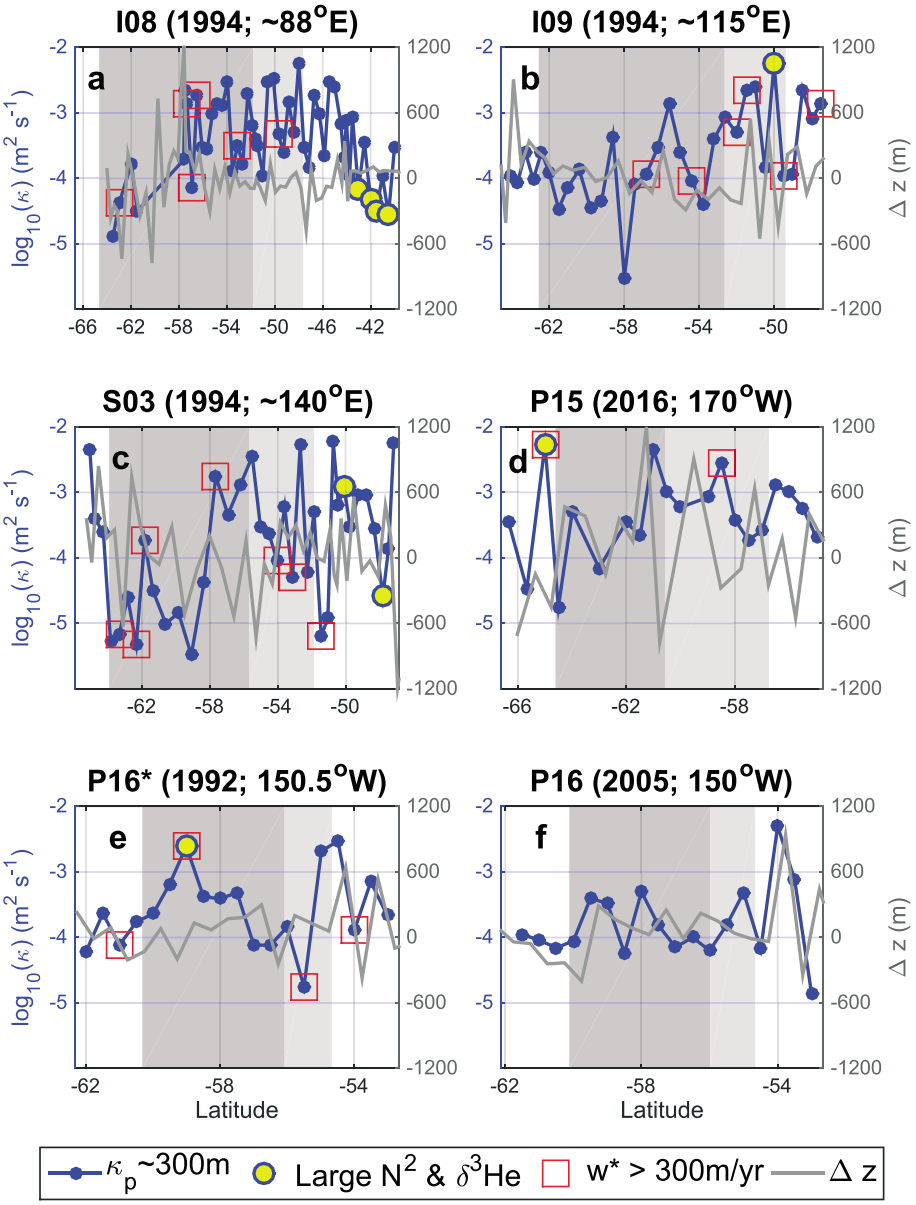

Figure 3. The maximum vertical diffusivity (κ; m^2/s; blue) 300 to 500 m above the ocean floor across six transects. Blue dots indicate where data are available for κ. Overlaid yellow dots indicate latitudes where near-floor N^2 is greater than 0.12×10^{-5} s^{-2} and δ^3He is greater than 10% from Figure 2, thus indicating where hydrothermal heat influences stratification and κ. Red squares indicate where upwelling within 300 m of the sea floor is greater than 300 m/year. Gray curves indicate the meridional change in bathymetry (z), where positive indicates a shoaling. The dark gray shaded region is the southern Antarctic Circumpolar Current boundary to the Polar Front, with the lighter gray shaded region the Polar Front to Sub-Antarctic Front.

significantly alter the background circulation but rather this hydrothermal heat flux must be released via convection (hydrothermal heat) to provide the largest impact.

The second key result regarding mixing is that the high vertical diffusivity values on I09, P15, and P16* in Figure 3 are an order of magnitude greater than found at locations just north or south of them, reinforcing the idea that hydrothermal activity has a localized impact in the ACC. This is also based on an assumption that hydrothermal input in the Southern Ocean is constant, given its detection at several locations (via helium signatures) since the 1970s (Downes et al., 2012).

The third key result is that the peak in κ (blue curve) and maxima in stratification associated with hydrothermal plumes (yellow dots) in Figure 3 also align with regions of high diapycnal upwelling ($w*$) within 500 m of the seabed. Interaction of the flow with topographic features can produce internal waves, and enhanced mixing where the waves break (Polzin et al., 1997), and increase local upwelling by an order of magnitude (Naveira Garabato et al., 2004; Waterhouse et al., 2014). This upwelling is dependent on the vertical diffusivity and stratification. We estimate the diapycnal upwelling rate ($w*$) along the six transects and find the average upwelling rate within 300 m of the sea floor is 10–50 m/year (Figure S2), which is in agreement with the ~30 m/year in the LCDW layer in the hydrothermally active and topographically rough southeast Atlantic region (Naveira Garabato et al., 2007). However, there are several data points where the upwelling exceeds this average by an order of magnitude or more (red squares in Figure 3).

The P15 and P16* transects each contain a data point where the upwelling maxima aligns with high vertical mixing, large stratification, and large δ^3He. No upwelling maxima are found along the 2005 P16 transect. Along I09, the third transect with a hydrothermal source within the ACC, there is no upwelling maxima aligned with the large stratification and large δ^3He within 300 m of the seafloor (yellow dot in Figure 3). This is because the upwelling maxima for this transect occurs in the depth range of 300 to 500 m above the sea floor (black curve at 50° S in Figure S2b).

We do not find evidence that hydrothermal plumes north of the ACC enhance local vertical mixing and upwelling. This is likely because the ACC region provides several conditions that enhance the impact of hydrothermal plumes: (1) an upwelling regime that increases plume rise height, (2) isopycnal mixing transports the plume to greater height, given that the isopycnals slope upward from the seafloor, (3) a large isopycnal tilt and poleward flow of deep waters, and (3) intersection with several mid-ocean ridge systems (Figure 1a). No other location has these conditions operating simultaneously.

4. Summary and Discussion

Numerous model studies have shown that conductive geothermal heat flux has a significant influence on ocean circulation. Our study, using a compilation of chemical and physical tracer data from the 1970s to present, shows that hydrothermal heat flux influences localized mixing in the ACC region greater than geothermal heat (Figure 4). Hydrothermal heat reduces stratification above the vent source and increases it to the south (associated with the background isopycnal tilt). The increase in stratification enhances vertical mixing and increases upwelling by an order of magnitude where the ACC encounters active vents on the mid-ocean ridge (Figures 2 and 3). In short, we hypothesize that hydrothermal heat released via vents located within the ACC region is a mechanism for mixing and upwelling hot spots in the ACC and has a strong influence on the local circulation, namely, within 500 m of the seabed sources.

Coherent stratification and mixing anomalies are found at several locations where the ACC crosses mid-ocean ridges. These anomalies extend as much as 500 m above the sea floor, in contrast to several recent studies (Ferrari et al., 2016; McDougall & Ferrari, 2017) that assume geothermal heating only impacts diapycnal upwelling in the bottom boundary layer, a layer tens of meters thick where the turbulent density flux is transported into the ocean floor, and not the stratified mixing layer above that is hundreds of meters thick. However, these studies do not take into account the effect of convective mixing by *hydrothermal* heat. Here we show that hydrothermal heating increases upwelling by up to an order of magnitude within 300 m, or even 500 m, of the seabed. While the diapycnal diffusivity above the bottom boundary layer due to the conductive geothermal heat flux is estimated as $\sim O(10^{-4})$ m/s^2 (Emile-Gaey & Madec, 2009; McDougall & Ferrari, 2017), we find diapycnal diffusivities of approximately 5×10^{-3} m/s^2 within 500 m of the seabed associated with hydrothermal heating and the associated changes in stratification (Figure 3).

Understanding and quantifying small-scale mixing in the deep ocean is vital for accurate representation of deep and bottom water mass circulation pathways and transformation. This study is the first attempt at quantifying the contribution of hydrothermal heat to deep mixing across several locations in the ACC. It has recently been suggested that omission of geothermal heating is a source of error in accurately quantifying decadal temperature trends along the ocean floor (Wunsch & Heimbach, 2014). Based on our new findings across the Southern Ocean, convective hydrothermal heat plays a significantly larger role in influencing local circulation than the conductive geothermal heat, and further work on quantifying the global impact of these seabed heat sources on upwelling is needed. Hydrothermal heat and geothermal heat need to be

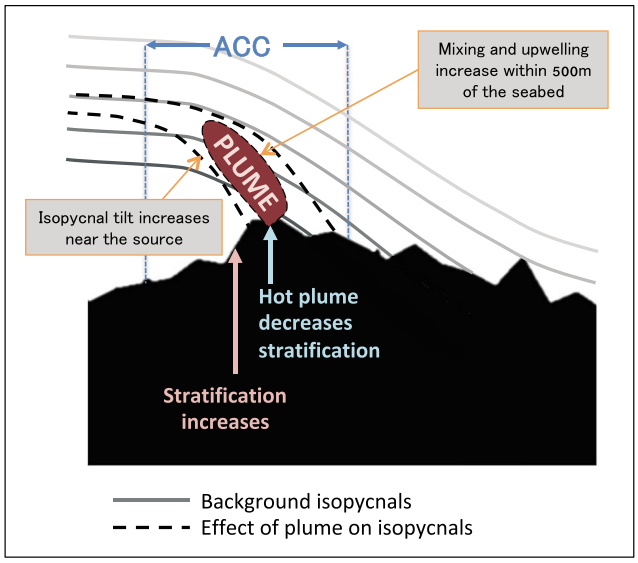

Figure 4. A summary of how hydrothermal heating and hydrothermal plumes influence the local circulation. The hydrothermal vent expels hot fluid into the ocean floor, weakening the local stratification, and the already steep isopycnal tilt (gray isopycnals) is enhanced within the latitude range of the high hydrothermal/geothermal heat and within the Antarctic Circumpolar Current (ACC; black dashed isopycnals). A sharp increase in stratification results just south of the plume source. The increased stratification results in an increase in the local vertical diffusivity and diapycnal upwelling by up to an order of magnitude compared to adjacent latitudes.

taken into account in modeling and observational-based (Garrett & Kunze, 2007; Nikurashin & Ferrari, 2011) studies as a source of deep ocean mixing. Given the small spatial scale of hydrothermal vent systems, direct observations of the impact of hydrothermal plumes on ocean circulation and mixing are challenging. However, hydrothermal activity can be sampled using appropriate chemical tracers at high spatial resolution (e.g., helium and manganese) and fine-scale CTD measurements, with a focus along topographic features and particularly mid-ocean ridges.

Acknowledgments
The authors would like to thank C. Wilkinson for processing and analyzing the recent P15 (2016) helium samples. All transect data were extracted from the CLIVAR and Carbon Hydrographic Office (CCHDO; https://cchdo.ucsd.edu/), and the data were analyzed using Python, Matlab, and Ocean Data View (https://odv.awi.de/). The geothermal heat flux estimates were taken from Davies and Davies (2010). S. M. D. was supported by the Australian Governments Business Cooperative Research Centres Programme through the Antarctic Climate and Ecosystems Cooperative Research Centre (ACE CRC). B. M. S. and S. R. R. received support from the Centre for Southern Hemisphere Oceans Research, a collaboration between CSIRO and the Qingdao National Laboratory for Marine Science and Technology.

References

Adcroft, A., Scott, J. R., & Marotzke, J. (2001). Impact of geothermal heating on the global ocean circulation. *Geophysical Research Letters*, *28*(9), 1735–1738.

Anderson, R. N., Langseth, M. G., & Sclater, J. G. (1977). The mechanisms of heat transfer through the floor of the Indian Ocean. *Journal of Geophysical Research*, *82*(23), 3391–3409.

Baker, E. T. (2017). Exploring the ocean for hydrothermal venting: New techniques, new discoveries, new insights. *Ore Geology Reviews*, *86*, 55–69.

Baker, E. T., Chadwick, C. C. Jr., Cowen, J. P., Dziak, R. P., Rubin, K. H., & Fornari, D. J. (2012). Hydrothermal discharge during submarine eruptions: The importance of detection, response, and new technology. *Oceanography*, *25*, 128–141.

Baker, E. T., German, C. R., & Elderfield, H. (1995). Hydrothermal plumes over spreading-center axes: Global distributions and geological inferences. In S. E. Humphris, et al. (Eds.), *Seafloor hydrothermal systems: Physical, chemical, biological, and geological interactions, Geophysical Monograph* (Vol. 91, pp. 47–71). Washington, D. C.: AGU.

Barnes, J. M., Morales Maqueda, M. A., Polton, J. A., & Megann, A. P. (2017). Idealised modelling of ocean circulation driven by conductive and hydrothermal fluxes at the seabed. *Ocean Modelling*, *122*, 26–35.

Bemis, K. G., von Herzen, R. P., & Mottl, M. J. (1993). Geothermal heat flux from hydrothermal plumes on the Juan de Fuca Ridge. *Journal of Geophysical Research*, *98*(B4), 6351–6365.

Chidichimo, M. P., Donohue, K. A., Watts, D. R., & Tracey, K. L. (2014). Baroclinic transport time series of the Antarctic Circumpolar Current measured in Drake Passage. *Journal of Physical Oceanography*, *44*(7), 1829–1853.

Clarke, W. B., Beg, M. A., & Craig, H. (1970). Excess helium 3 at the North Pacific Geosecs station. *Journal of Geophysical Research*, *75*(36), 7676–7678.

Cunningham, S. A., Alderson, S. G., King, B. A., & Brandon, M. A. (2003). Transport and variability of the Antarctic Circumpolar Current in Drake Passage. *Journal of Geophysical Research*, *108*(C5), 8084.

Davies, J. H., & Davies, D. R. (2010). Earth's surface heat flux. *Solid Earth*, *1*, 5–24.

de Lavergne, C., Madec, G., Le Sommer, J., Nurser, A. J. G., & Naveira Garabato, A. C. (2016). On the consumption of antarctic bottom water in the abyssal ocean. *Journal of Physical Oceanography*, *46*, 635–661.

Downes, S. M., Hogg, A. M., Griffies, S. M., & Samuels, B. L. (2016). The transient response of southern ocean circulation to geothermal heating in a global climate model. *Journal of Climate*, *29*, 5689–5708.

Downes, S. M., Key, R. M., Orsi, A. H., Speer, K. G., & Swift, J. H. (2012). Tracing Southwest Pacific Bottom Water using potential vorticity and helium-3. *Journal of Physical Oceanography*, *42*(12), 2153–2168.

Emile-Gaey, J., & Madec, G. (2009). Geothermal heating, diapycnal mixing and the abyssal circulation. *Ocean Science*, *5*, 203–217.
Ferrari, R., Mashayek, A., McDougall, T. J., Nikurashin, M., & Campin, J.-M. (2016). Turning ocean mixing upside down. *Journal of Physical Oceanography*, *46*, 2239–2261.
Garrett, C., & Kunze, E. (2007). Internal tide generation in the deep ocean. *Annual Review of Fluid Mechanics*, *39*, 57–87.
Gnanadesikan, A., Pradal, M.-A., & Abernathy, R. (2015). Exploring the isopycnal mixing and helium-heat paradoxes in a suite of Earth system models. *Ocean Science*, *11*, 591–605.
Haase, K. M., Petersen, S., Koschinsky, A., Seifert, R., Devey, C. W., Keir, R., et al. (2009). Fluid compositions and mineralogy of precipitates from Mid Atlantic Ridge hydrothermal vents at 4° 48′ s. PANGAEA. https://doi.org/10.1594/PANGAEA.727454
Hahm, D., Baker, E. T., Rhee, T. S., Won, Y.-J., Resing, J. A., Lupton, J. E., et al. (2015). First hydrothermal discoveries on the Australian-Antarctic Ridge: Discharge sites, plume chemistry, and vent organisms. *Geochemistry, Geophysics, Geosystems*, *16*, 3061–3075. https://doi.org/10.1002/2015GC005926
Hamza, V., Cardoso, R., & Neto, P. C. (2008). Spherical harmonic analysis of the Earth's conductive heat flow. *International Journal of Earth Sciences*, *97*, 205–226.
Heywood, K. J., Naveira Garabato, A. C., & Stevens, D. P. (2002). High mixing rates in the abyssal Southern Ocean. *Nature*, *415*, 1011–1014.
Hofmann, M., & Morales Maqueda, M. A. (2009). Geothermal heat flux and its influence on the oceanic abyssal circulation and radiocarbon distribution. *Geophysical Research Letters*, *36*, L03603. https://doi.org/10.1029/2008GL036078
Jackett, D., & McDougall, T. J. (1997). A neutral density variable for the world's oceans. *Journal of Physical Oceanography*, *27*, 237–263.
Krylov, A. Y., Mamryrin, B. A., Khabarin, L. A., Mazina, T. I., & Silin, Y. I. (1974). Helium isotopes in ocean floor bedrock. *Geokhimiya*, *8*, 1220–1225.
Kunze, E., Firing, E., Hummon, J. M., Chereskin, T. K., & Thurnherr, A. M. (2006). Global abyssal mixing inferred from lowered ADCP shear and CTD strain profiles. *Journal of Physical Oceanography*, *36*, 1553–1575.
Lupton, J. (1998). Hydrothermal helium plumes in the Pacific Ocean. *Journal of Geophysical Research*, *103*(C8), 15,853–15,868.
Lupton, J. E., Baker, E. T., & Massoth, G. J. (1999). Helium, heat, and the generation of hydrothermal event plumes at mid-ocean ridges. *Earth and Planetary Science Letters*, *171*, 343–350.
Lupton, J. E., & Craig, H. (1975). Excess ^{3}He in oceanic basalts: Evidence for terrestrial primordial helium. *Earth and Planetary Science Letters*, *26*, 133–139.
Lupton, J. E., Pyle, D. G., Jenkins, W. J., Greene, R., & Evans, L. (2004). Evidence for an extensive hydrothermal plume in the Tonga-Fiji region of the South Pacific. *Geochemistry, Geophysics, Geosystems*, *5*, Q01003. https://doi.org/10.1029/2003GC000607
Mashayek, A., Ferrari, R., Vettoretti, G., & Peltier, W. R. (2013). The role of the geothermal heat flux in driving the abyssal ocean circulation. *Geophysical Research Letters*, *40*, 3144–3149. https://doi.org/10.1002/grl.50640
McDougall, T. J., & Ferrari, R. (2017). Abyssal upwelling and downwelling driven by near-boundary mixing. *Journal of Physical Oceanography*, *47*, 261–283.
Naveira Garabato, A. C., Polzin, K. L., King, B. A., Heywood, K. J., & Visbeck, M. (2004). Widespread intense turbulent mixing in the Southern Ocean. *Science*, *303*, 210–213.
Naveira Garabato, A. C., Stevens, D. P., Watson, A. J., & Roether, W. (2007). Short-circuiting of the overturning circulation in the antarctic circumpolar current. *Nature*, *447*, 194–197.
Nikurashin, M., & Ferrari, R. (2011). Global energy conversion rate from geostrophic flows into internal lee waves in the deep ocean. *Geophysical Research Letters*, *38*, L08610. https://doi.org/10.1029/2011GL046576
Piecuch, C. G., Heimbach, P., Ponte, R. M., & Forget, G. (2015). Sensitivity of contemporary sea level trends in a global ocean state estimate to effects of geothermal fluxes. *Ocean Modelling*, *96*, 214–220.
Polzin, K. L., Toole, J. M., Ledwell, J. R., & Smith, R. W. (1997). Spatial variability of turbulent mixing in the abyssal ocean. *Science*, *276*, 93–96.
Rintoul, S. R. (2018). The global influence of localized dynamics in the Southern ocean. *Nature*, *558*, 209–218.
Rintoul, S. R., & Naveira Garabato, A. C. (2013). Chapter 18—Dynamics of the Southern Ocean circulation. In G. Siedler, et al. (Eds.), *Ocean circulation and climate a 21st century perspective, International Geophysics* (Vol. 103, pp. 471–492). Oxford: Academic Press.
Rüth, C., Well, R., & Roether, W. (2000). Primordial ^{3}He in south atlantic deep waters from sources on the Mid-Atlantic Ridge. *Deep-Sea Research Part I*, *47*, 1059–1075.
Saito, M. A., Noble, A. E., Tagliabue, A., Goepfert, T. J., Lamborg, C. H., & Jenkins, W. J. (2013). Slow-spreading submarine ridges in the South Atlantic as a significant oceanic iron source. *Nature Geoscience*, *6*, 775–779.
Sloyan, B. M. (2005). Spatial variability of mixing in the Southern Ocean. *Geophysical Research Letters*, *32*, L18603. https://doi.org/10.1029/2005GL023568
Sloyan, B. M. (2006). Antarctic bottom and lower circumpolar deep water circulation in the eastern Indian Ocean. *Journal of Geophysical Research*, *111*, C02006. https://doi.org/10.1029/2005JC003011
Speer, K. G., & Helfrich, K. R. (1995). Hydrothermal plumes: a review of flow and fluxes. *Geological Society*, *87*, 373–385.
Srinivasan, A., Top, Z., Schlosser, P., Hohmann, R., Iskandarani, M., Olson, D. B., et al. (2004). Mantle ^{3}He distribution and deep circulation in the Indian Ocean. *Journal of Geophysical Research*, *109*, C06012. https://doi.org/10.1029/2003JC002028
Veirs, S. R., McDuff, R. E., Lilley, M. D., & Delaney, J. R. (1999). Locating hydrothermal vents by detecting buoyant, advected plumes. *Journal of Geophysical Research*, *104*(B12), 29,239–29,247.
Waterhouse, A. F., MacKinnon, J. A., Nash, J. D., Alford, M. H., Kunze, E., Simmons, H. L., et al. (2014). Global patterns of diapycnal mixing from measurements of the turbulent dissipation rate. *Journal of Physical Oceanography*, *44*, 1854–1872.
Well, R., Lupton, J., & Roether, W. (2001). Crustal helium in deep pacific waters. *Journal of Geophysical Research*, *106*(C7), 14,165–14,177.
Well, R., Roether, W., & Stevens, D. P. (2003). An additional deep-water mass in drake passage as revealed by ^{3}He data. *Deep Sea Research Part I*, *50*, 1079–1098.
Winckler, G., Newton, R., Schlosser, P., & Crone, T. J. (2010). Mantle helium reveals Southern Ocean hydrothermal venting. *Geophysical Research Letters*, *37*, L05601. https://doi.org/10.1029/2009GL042093
Wunsch, C., & Heimbach, P. (2014). Bidecadal thermal changes in the abyssal ocean. *Journal of Physical Oceanography*, *44*, 2013–2030.